Multisubband photoluminescence in *p*-type modulation-doped $Al_xGa_{1-x}N/GaN$ superlattices

Erik L. Waldron* and E. Fred Schubert†
Center for Photonics Research, 8 Saint Mary's Street, Boston University, Boston, Massachusetts 02215

Amir M. Dabiran
SVT Associates, 7620 Executive Drive, Eden Prarie, Minnesota 55344

(Received 20 June 2002; published 31 January 2003)

Photoluminescence spectra from *p*-type modulation-doped $Al_{0.20}Ga_{0.80}N/GaN$ superlattices with 10-nm well width show multiple, well resolved, interband transitions between quantum-confined states. In addition to the ground-state transition, a number of excited-state transitions are observed. The observation of multiple peaks is attributed to the inverse dependence of subband population and oscillator strength on energy. The relative strength of the peaks strongly changes with excitation intensity. At low excitation intensity, the spectra display only the ground-state transition. At higher excitation intensity, excited-state transitions become dominant. At high excitation intensities, the dominant transition occurs at energies about 500 meV above the electron ground-state to hole ground-state transition. Self-consistent calculations are used to assign transition energies, lifetimes, and rates to each photoluminescence line. Theoretical and experimental transition energies are in excellent agreement. We attribute the excellent optical properties to the modulated doping of the structure, which consists of doped barriers and undoped well layers. Our calculations also show an average recombination lifetime of 50 ns at high excitation intensities, despite the large quantum-confined Stark effect. The changes of the photoluminescence spectra can be explained via the effects of band filling and oscillator strengths at higher excitation intensity.

DOI: 10.1103/PhysRevB.67.045327 PACS number(s): 78.67.De, 73.21.Cd, 73.20.At, 78.55.Cr

The role of spontaneous and piezoelectric fields[1–3] in the $Al_xGa_{1-x}N$ material system continues to receive great interest due to the influence of these fields on both the optical[4,5] and electronic[6–8] properties of $Al_xGa_{1-x}N$ heterostructures. In particular, as III-nitride optical devices approach the ultraviolet (UV) range, the use of $Al_xGa_{1-x}N/GaN$ and $Al_xGa_{1-x}N/Al_yGa_{1-y}N$ quantum wells (QW's) is becoming a necessity. However, the recombination efficiency of these QW's has been shown to be very inefficient for wider well sizes due to the spatial separation of the electron and hole wave functions.[9,10] This separation is due to the strong polarization fields present in $Al_xGa_{1-x}N$ QW's. The luminescence emitted from these QW's is also strongly redshifted due to the quantum-confined Stark effect (QCSE).[11]

$Al_xGa_{1-x}N/GaN$ *p*-type superlattices (SL's) are of great interest because of their enhanced *p*-type doping properties.[12,13] Specifically, modulation-doped SL's demonstrate low-temperature electrical properties superior to any *p*-type $Al_xGa_{1-x}N/GaN$ material reported to date.[6] The modulation-doped SL investigated presently, which is the same modulation-doped SL as in Ref. 6, has a resistivity of 0.068 Ω cm, a mobility of 36 $cm^2/V\,s$, and a free hole concentration of 2.5×10^{18} cm^{-3}, all measured at 90 K. Because of the effects of superlattice and piezoelectric doping, the free carrier concentration is nearly independent of temperature.

In this work we report the first experimental results on multisubband photoluminescence (PL) spectra of *p*-type modulation-doped $Al_{0.20}Ga_{0.80}N/GaN$ SL's. We observe clearly resolved multisubband luminescence peaks whose relative intensity changes with excitation intensity. The luminescence peak energies are compared to the transition energies calculated from a self-consistent Poisson-Schrödinger one-dimensional (1D) solver using the method of finite differences. In addition, spontaneous recombination rates and lifetimes are compared between experiment and theory by using the calculated energies and envelope functions. The theoretical and experimental results agree very well. The oscillator strength and population distribution between subbands have opposite dependencies on energy. As the electronic eigenstate energy increases so does the overlap integral between the electronic eigenstate and the ground hole eigenstate. However, the carrier population in the higher energy electronic subbands decreases. As a result, spontaneous transitions between sparsely populated electronic excited states and the ground hole state become observable at high excitation intensity due to the larger overlap integral between higher-energy electron-hole pair states. These characteristics are due to the large polarization fields present in the SL. The polarization fields also destroy the symmetry of the QW's and therefore remove all parity selection rules between transitions.

Figure 1 shows a schematic and the self-consistently calculated band diagram of the Ga-faced $Al_{0.20}Ga_{0.80}N/GaN$ SL sample under study. The SL samples were grown on a *c*-plane sapphire substrate by molecular beam epitaxy (MBE). The SL's are doped with Mg at a level of $N_{Mg}\approx1\times10^{19}$ cm^{-3}. One of the SL's is uniformly doped and the other is modulation doped. The modulation-doped SL has only the barrier layers doped whereas the well layers are undoped. The uniformly doped sample displays one broad PL line that we attribute to electron subband to neutral acceptor transitions. The free holes in the modulation-doped SL

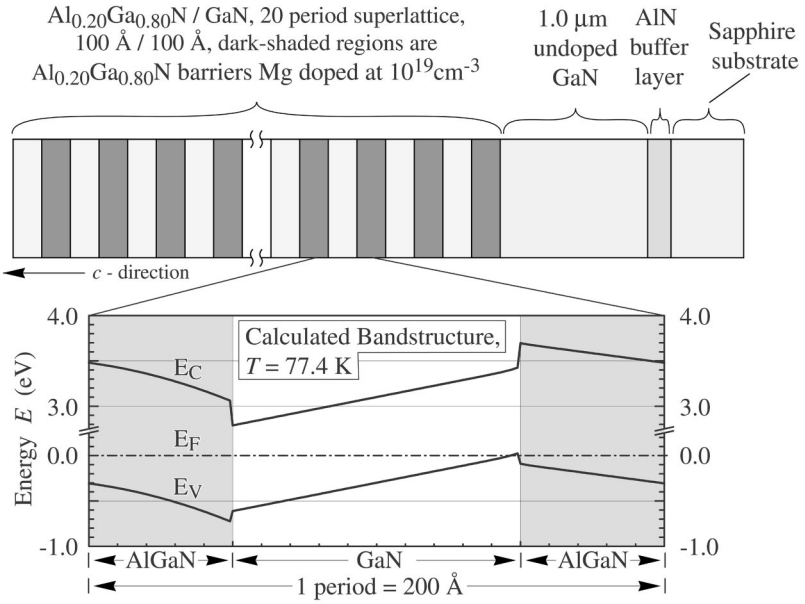

FIG. 1. (a) Schematic of the $Al_{0.20}Ga_{0.80}N$/GaN superlattice used in this study. (b) Self-consistently calculated band diagram.

are measured at $\approx 2.5\times 10^{18}$ cm^{-3} at low temperature. The modulation-doped SL has 20 periods with equal barrier and well widths of 100 Å. The SL layers are below the critical thickness and were grown pseudomorphically on a GaN buffer layer, resulting in biaxial tensile strain in the barrier layers.[14] The 325-nm (3.815 eV) line of a He-Cd laser was used for excitation and the PL was dispersed with a 0.75-m spectrometer in the Czerny-Turner configuration and a Raleigh resolving power of ~2000. The SL was cooled using the coldfinger of a liquid-nitrogen cryostat. The detection used standard lock-in techniques in conjunction with a GaAs photodetector.

SL structures use semiconductors with different band gaps and, in the case of the III-nitrides, large internal polarization fields.[15,16] A bound surface charge results when $\mathbf{P}\cdot\hat{n}\neq 0$, where $\mathbf{P}$ is the total polarization at the surface and $\hat{n}$ is the surface normal unit vector. A bound interface charge results when $\nabla\cdot\mathbf{P}\neq 0$, where $\mathbf{P}$ is the total internal polarization. The total polarization is just the sum of the piezoelectric and the spontaneous polarization, i.e., $\mathbf{P}=\mathbf{P}_{\rm pz}+\mathbf{P}_{\rm sp}$. The quantity $\mathbf{P}_{\rm pz}$ can be calculated using[17]

$$P_{i,\rm pz}=e_{ijk}\epsilon_{jk}, \tag{1}$$

where e_{ijk} are the piezoelectric constants, ϵ_{jk} is the general strain tensor, and $i, j, k=1, 2, 3$ are the three principal axes. Due to the symmetry of the wurtzite structure Eq. (1) can be rewritten more conveniently from tensor to matrix form

$$P_{i,\rm pz}=e_{ij}\epsilon_j, \tag{2}$$

where $i=1, 2, 3$ and $j=1, 2, 3, 4, 5, 6$. Because the piezoelectric tensor of wurtzite has only three nonvanishing independent components, e_{33}, e_{13}, and e_{15}, and we may safely neglect shear strain, $\epsilon_4=\epsilon_5=\epsilon_6=0$, we simply get

$$P_{z,\rm pz}=e_{31}(\epsilon_x+\epsilon_y)+e_{33}\epsilon_z. \tag{3}$$

We use $e_{31}=-0.49$ C/m^2, $e_{33}=0.73$ C/m^2,[15] and assume a Vegard relationship between the spontaneous polarization in GaN and AlN, $P_{z,\rm sp}=(-0.029-0.052x)$ C/m^2, x being the molar fraction of Al ($0\leqslant x\leqslant 1$). We neglect any nonlinearity in piezoelectric polarization due to the small deviation from linearity for AlGaN on relaxed GaN.[18]

The SL band diagram is calculated by solving the Poisson-Schrödinger system of equations self-consistently using the method of finite differences. We use a simple phenomenological model where we consider a twofold degenerate valence band consisting of heavy and light holes of the same isotropic effective mass. The eigenenergies ε_l^i and envelope eigenfunctions $\psi_l^i(z)$ of the electron and hole subbands are calculated from the 1D effective-mass Schrödinger equation

$$\left[-\frac{\hbar^2}{2}\frac{d}{dz}\frac{1}{m_l^*(z)}\frac{d}{dz}+V_l(z)\right]\psi_l^i(z)=\varepsilon_l^i\psi_l^i(z), \tag{4}$$

where we use an $Al_xGa_{1-x}N$ heavy and light hole mass[16] of $m_v=(1.76+1.77x)m_0$ (m_0 is the free-electron mass), electron mass[19] of $m_c=(0.228)m_0$, valence-band discontinuity[18] of $\Delta E_h=(0.27)\Delta E_g$, and temperature-dependent energy gap[20] of $E_g(T,x)=[E(0)-\alpha T^2/(\beta+T)]$, where $E(0)=3.487$ eV, $\alpha=12.85\times 10^{-4}$ eV/K, and $\beta=1235$ K. The potential energy is given by

$$V_l(z)=\Delta E_l+q_l\phi(z). \tag{5}$$

In the above equations, l labels the conduction or valence band, i labels the subband within l, and ΔE_l are the band-edge discontinuities. The term $\phi(z)$ on the right-hand side of Eq. (5) is the electrostatic potential resulting from all charges in the system,

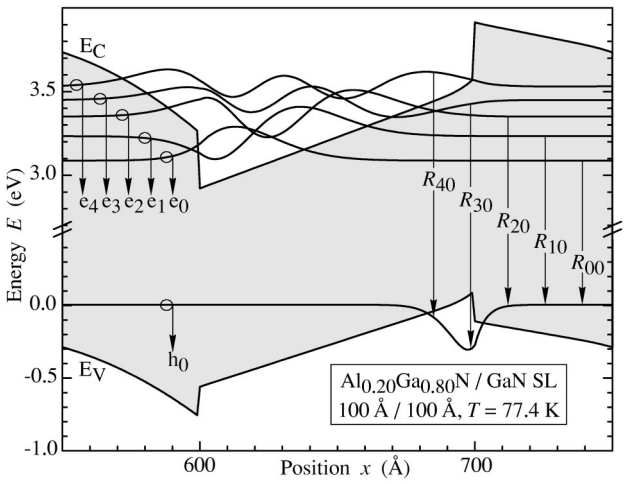

FIG. 2. Self-consistently calculated band diagram showing the conduction band, valence band, and eigenfunctions of the 1D effective-mass Schrödinger equation.

$$\frac{d^2}{dz^2}\phi(z) = -\frac{q[n_h(z) - n_e(z) + N_D^+(z) - N_A^-(z)] + \rho_{\text{pol}}(z)}{\epsilon_r \epsilon_0}, \tag{6}$$

where q is the magnitude of the electronic charge, $N_D^+(z)$ is the concentration of ionized donors, $N_A^-(z)$ is the concentration of ionized acceptors, $\rho_{\text{pol}}(z)$ is the bound polarization charge which is present at each SL interface, and the relative dielectric constant along $\hat{z}$, $\epsilon_r = 10.4$, is taken as constant throughout the structure. The free-electron and free hole concentrations are given by Fermi-Dirac statistics,

$$n_l(z) = N_l \sum_i |\psi_l^i(z)|^2 \ln[1 + \epsilon^{(\varepsilon_F - \varepsilon_l^i)/(kT)}], \tag{7}$$

where ε_F is the Fermi energy, and $N_l = m_l^* kT/\pi\hbar^2$.

Figure 2 shows the self-consistently calculated band diagram as well as the eigenfunctions used for the quantum-confined transition data. We choose the first five electronic eigen-states and the ground hole eigenstate for our transition data. The transitions, labeled on the right side of the figure, between these chosen eigenfunctions cover the energy range of experimentally observed transitions with excellent agreement. The figure also shows the band tilting due to the large polarization field resulting primarily from the bound interface charges. The internal electric field is slightly greater than 0.6 MV/cm. This field causes the electron and hole eigenfunctions to separate markedly along the growth direction (QCSE). It can also be seen in the figure that the higher energy electron states have a greater overlap with the ground hole state h_0 as compared to the lower energy electron states. This overlap dependence on energy will be quantified below.

It should be noted that our one-dimensional model is based on an ideal SL with perfectly abrupt interfaces. There are, however, many physical effects that induce disorder in AlGaN/GaN multiple quantum well structures. These effects include impurity disorder, well-thickness variations, lattice imperfections, compositional fluctuations, strain fluctuations, and the resulting piezoelectric field fluctuations, and other effects. Capacitance-voltage (C-V) measurements on our SL samples have clearly shown multiple hole gases. Individual peaks of the C-V profiles show a full width at half maximum of only 30 Å.[6] Such narrow profiles indicate a high superlattice interfacial quality and planar growth over a large area. Additionally, the hole mobilities and resistivities of our AlGaN/GaN heterostructures are 36 $\text{cm}^2/\text{V s}$ and 0.068 Ω cm at 90 K,[6] indicating excellent interfacial quality. This is consistent with the results of other groups[21,22] who concluded that the interfacial quality of their AlGaN/GaN heterostructures was excellent based on PL data. We therefore attribute the multiple peaks found in PL measurements to multisubband transitions. Disorder effects, although indisputably present, are believed to be secondary.

Using the 1D band diagram we calculate the spontaneous recombination rates taking place in the quantum well. We begin with the general expression for direct transitions between states in a III-V semiconductor,[23]

$$R_{\text{total}} = \sum_{i,j} R_{ij}(h\nu) = \sum_{i,j} \int_{E_{ij}}^{\infty} Z(h\nu) B_{ij}(h\nu) f_c(h\nu)[1 - f_v(h\nu)] \rho_{\text{red}} d(h\nu), \tag{8}$$

where

$$Z(h\nu) \approx \frac{8\pi}{(hc)^3} \mu^3 (h\nu)^2, \tag{9}$$

$$B_{ij}(h\nu) = \frac{e^2}{2m_0^2 \epsilon_0 \mu^2 \nu} |M_{ij}|^2, \tag{10}$$

M_{ij} being the momentum matrix element. M_{ij} is given in the dipole approximation ($e^{-i\mathbf{k}_{op}\cdot\mathbf{r}} \approx 1$) for incident light whose optical electric field is perpendicular to the SL growth axis[24] by

$$|M_{ij}|^2 \approx \frac{m_0^2 E_{ij}}{3m_c} \frac{1 + \Delta/E_{ij}}{1 + 2\Delta/3E_{ij}} \left| \int_{-\infty}^{\infty} \phi_{v,j}^*(z) \phi_{c,i}(z) dz \right|^2, \tag{11}$$

f_c is the probability that the higher energy state is occupied, f_v is the probability that the lower energy state is occupied. The reduced density of states is given by

$$\rho_{\text{red}} = \left(\frac{1}{\rho_c} + \frac{1}{\rho_v} \right)^{-1}, \tag{12}$$

where

$$\rho_c = \frac{m_c}{\pi\hbar^2 L_z} \tag{13}$$

and

$$\rho_v = \frac{2m_v}{\pi\hbar^2 L_z}. \tag{14}$$

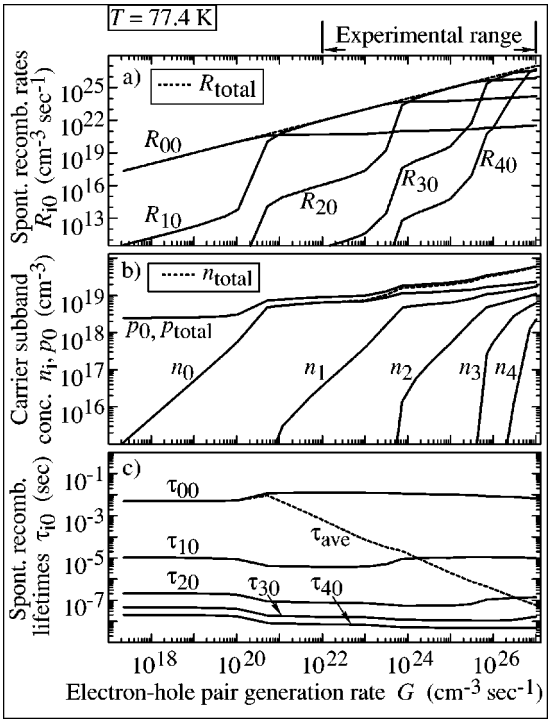

FIG. 3. Calculated (a) spontaneous recombination rates, (b) carrier subband concentrations, and (c) spontaneous recombination lifetimes for a *p*-type modulation-doped $Al_{0.20}Ga_{0.80}N/GaN$ SL.

Equations (13) and (14) are the two-dimensional density of states divided by L_z ($L_z = 200$ Å is the period of the SL) for the conduction band and valence band, respectively. The factor of 2 in Eq. (14) accounts for the twofold degenerate valence band we use in our model.

In Eq. (8) through Eq. (14), e, m_0, m_v, m_c are as given earlier, ν is the frequency of the emitted photon, c is the speed of light in vacuum, μ is the index of refraction of the semiconductor, E_{ij} is the transition energy between the ith electronic subband and the jth hole subband, $\phi_{v,j}$ and $\phi_{c,i}$ are the envelope functions corresponding to E_{ij}, and $\Delta = 0.040$ eV is the crystal-field split-off energy.

To obtain the envelope functions we self-consistently solve for the first 40 electronic and hole eigenstates in a seven QW structure. We then take the first five electronic eigenstates and the ground hole eigenstate in the central QW. We note that the first one or two QW's near the surface of a SL typically do not support bound states due to the combined effects of the polarization field and Fermi-level pinning. We neglect this minor effect and assume all wells in the SL behave identically. Once the envelope functions and eigenenergies are calculated we can easily obtain both the overlap integrals and transition energies, allowing us to calculate the spontaneous transition rate per unit volume between any electron subband to hole subband pair, R_{ij}.

Figure 3 shows calculated spontaneous recombination rates, carrier subband concentrations, and spontaneous recombination lifetimes of the $Al_{0.20}Ga_{0.80}N/GaN$ SL covering ten orders of magnitude in pump intensity. Figure 3(a) shows the increase of the spontaneous recombination rates R_{i0} between the ith electronic subband and the ground hole subband as G is increased. The R_{i0} increase sharply as the electron quasi-Fermi level approaches the ith electronic subband energy from below. Once the electron quasi-Fermi level gets $\approx 2kT$ above the ith electronic subband energy, R_{i0} begins to level off. Thus the particular value of G at which R_{i0} begins to level off corresponds to the electron quasi-Fermi level rising into the ith electronic subband. This agrees qualitatively with our PL data.

TABLE I. Theoretically calculated values using Eqs. (8)–(15) and envelope functions shown in Fig. 2.

Transition	$\hbar\omega$ (eV)	$\tau_{i0,ave}$ (sec)	$\lvert\text{overlap}\rvert^2$
$e_0 \rightarrow h_0$	3.082	$\tau_{00,ave} = 9.3\times10^{-3}$	3.2×10^{-7}
$e_1 \rightarrow h_0$	3.228	$\tau_{10,ave} = 8.2\times10^{-6}$	1.5×10^{-4}
$e_2 \rightarrow h_0$	3.345	$\tau_{20,ave} = 1.1\times10^{-7}$	6.8×10^{-3}
$e_3 \rightarrow h_0$	3.444	$\tau_{30,ave} = 2.1\times10^{-8}$	3.1×10^{-2}
$e_4 \rightarrow h_0$	3.524	$\tau_{40,ave} = 9.1\times10^{-9}$	6.9×10^{-2}

Figure 3(b) displays the carrier subband concentrations as a function of G. At small values of G the total number of holes p_{total} approaches the equilibrium value due to doping, $p_{eq} = 2.5\times10^{18}$ cm^{-3}. As G is increased the electronic subbands begin to populate commensurate with their energies. At large values of G where $p_{total} \gg p_{eq}$, n_{total} approaches p_{total}.

Figure 3(c) clearly shows the decrease in the average spontaneous recombination lifetime as the electron-hole pair generation rate is increased. The average spontaneous recombination lifetime is given by

$$\tau_{ave}(G) = \frac{\Sigma_i n_i}{\Sigma_i \frac{n_i}{\tau_{i0}}} = \frac{n_{total}}{\Sigma_i \frac{n_i}{\tau_{i0}}} = \frac{n_{total}}{\Sigma_i R_{i0}}, \tag{15}$$

where n_i is the number of free electrons per unit volume in subband i, τ_{i0} is the electron subband to ground hole subband recombination lifetime, and R_{i0} is the electron subband to ground hole subband recombination rate given by Eq. (8). As G is increased, τ_{ave} decreases from $\tau_{ave} = 4.9\times10^{-3}$ sec at $G = 1\times10^{17}$ cm^{-3} sec^{-1}, down to $\tau_{ave} = 5.9\times10^{-8}$ sec at $G = 1\times10^{27}$ cm^{-3} sec^{-1}. Therefore as one increases G, a much smaller average recombination lifetime can be recovered despite the influence of the QCSE. Nonradiative transitions are neglected because of the low temperature.

Further inspection of Fig. 3(c) shows a slight dependence of the τ_{i0} on G, $\tau_{i0} = \tau_{i0}(G)$. This is due mainly to the dependence of τ on the Fermi occupation functions and the energy

$$\tau = n/R \propto \frac{\int f_c(h\nu)d(h\nu)}{\int (h\nu) f_c(h\nu)(1 - f_v(h\nu))d(h\nu)}, \tag{16}$$

which follows from Eqs. (8) and (15).

To determine the quasi-Fermi levels, and thus f_c and f_v, we assume unity quantum absorption efficiency at the pump laser energy, require charge neutrality, and equate the laser generation rate to the sum of subband recombination rates,

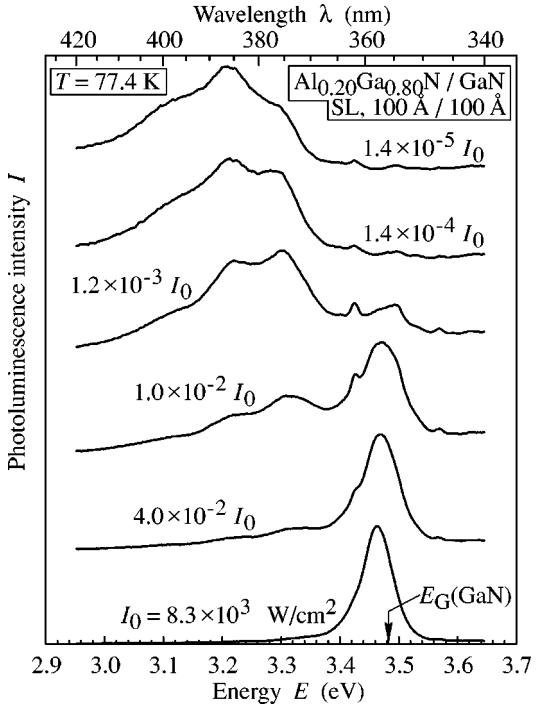

FIG. 4. PL spectra of a *p*-type modulation-doped $Al_{0.20}Ga_{0.80}N/GaN$ superlattice at different pump intensities covering five orders of magnitude. Luminescence peaks are clearly resolved over a nearly 500-meV range due to the combined effects of QCSE, band filling, and oscillator strengths.

$$\frac{dn}{dt}=G=\frac{P}{\hbar\omega_{\text{pump}}}\frac{\alpha}{\pi[r^2/\cos(\theta)]}=R_{\text{total}}=\sum_{i,j}R_{ij}, \quad (17)$$

where P is the pump laser power, $\hbar\omega_{\text{pump}}$ is the energy of the pump laser line, α is the absorption coefficient for the SL, $2r$ is the minor axis of the laser excitation spot on the sample surface, and θ is the angle between the laser beam and the sample normal. We measure $P=37$ mW, $\hbar\omega_{\text{pump}}=3.815$ eV, $\theta=45°$, and use $\alpha=1.2\times10^5$ cm^{-1}.[25] We use neutral density filters and vary r to achieve the desired intensity by defocussing the excitation spot, which is diffraction limited to $r\approx10$ μm. We calculate our laser intensity I to range from $I_{\text{max}}=8.3\times10^3$ W/cm^2 to $I_{\text{min}}=1.2\times10^{-1}$ W/cm^2. This corresponds to an electron-hole generation rate of $G_{\text{max}}\approx1\times10^{27}$ cm^{-3} sec^{-1} and $G_{\text{min}}\approx1\times10^{22}$ cm^{-3} sec^{-1}.

To further quantify our theoretical data, we calculate the transition energies, the average spontaneous recombination lifetimes, and the overlap inegrals squared, as shown in Table I. The data clearly shows the interplay of the overlap integral with the quantum-confined state population. Although the low-energy states are more populated than the high-energy states, their small overlap integral prevents their luminescence from dominating the PL spectrum. High-energy peaks are therefore visible at high pump intensities despite their lower carrier occupation.

Because one may write in general[26]

$$\tau=\frac{\tau_0}{\left|\int_{-\infty}^{\infty}\phi_v^*(z)\phi_c(z)dz\right|^2}, \quad (18)$$

where τ_0 corresponds to the minimum lifetime of a vertical transition, we see that since the $|\text{overlap}|^2$ covers roughly six orders of magnitude, so too do the spontaneous lifetimes of the various transitions. The longest average electron subband to hole ground state lifetime, $\tau_{i0,\text{ave}}$, we calculate is $\tau_{00,\text{ave}}=9.3$ ms for the ground-state to ground-state transition. However, even at the low electron-hole generation rate of $\approx7\times10^{24}$ cm^{-3} sec^{-1}, the average spontaneous lifetime τ_{ave} has a value of ≈3 μs. This is in excellent agreement with typical values in the literature[21] for a similar 100 Å $Al_{0.15}Ga_{0.85}N/GaN$ QW structure. The shortest average electron subband to hole ground-state lifetime we calculate is $\tau_{40,\text{ave}}=9.1$ ns. Using Eq. (18), this translates into a lifetime of $\approx$628 ps for transitions whose overlap integral approaches unity, as is the case for a much thinner ($\sim$15–25 Å) QW. This is also in good agreement[10,21] with typical lifetimes reported in the literature.

Figure 4 shows low-temperature PL spectra of the modulation-doped $Al_{0.20}Ga_{0.80}N/GaN$ SL covering five orders of magnitude in pump intensity. Five clearly resolved PL peaks are observed at $E\simeq3.11$, 3.21, 3.30, 3.42, and 3.46 eV. The figure has a rich structure displaying four main features. First, it can be clearly seen that there are multiple, well-resolved PL peaks which change in relative intensity as the pump intensity (maximum pump intensity$=I_{\text{max}}=I_0=8.3\times10^3$ W/cm^2) is changed. Second, not only are transitions well above the ground-state to ground-state transition seen, but remarkably, the high-energy transitions actually dominate the spectrum at high pump intensities. Third, the higher energy PL peaks increase in intensity relative to the lower energy PL peaks as the pump intensity is increased, in excellent agreement with the theory described earlier. Last, there is very little blueshifting of individual PL peaks as the pump intensity is increased.

We attribute the PL peaks to the sum of the individual Lorentzian broadened transitions between quantum-confined subband states in the conduction and valence band. The lack of appreciable blueshifting of individual PL peaks is consistent with a lack of screening. The lack of screening can be attributed to the fact that as the laser pump intensity is increased over our experimentally available range covering five orders of magnitude, the calculated average spontaneous lifetime decreases by roughly four orders of magnitude. Thus the steady-state number of electron-hole pairs per unit volume increases by only about one order of magnitude over our entire experimental pump intensity range. Therefore the amount of charge available to screen the internal polarization field begins to saturate at high pump intensities. This is due to two reasons. First, as the laser pump intensity is increased the average spontaneous lifetime decreases, tending to limit the number of electron-hole pairs generated. Second, as higher energy electron-hole pair states become populated their overlap integrals approach unity and they can no longer screen the internal polarization fields effectively. Both the

relatively small magnitude and the saturation of the blueshift has recently been reported in the literature for a similar QW structure.[27]

The expected strength of the GaN buffer layer peak is weak due to the much larger SL thickness (0.4 μm) as compared to the SL absorption length ($\alpha^{-1} \simeq 0.083$ μm, assuming $\alpha = 1.2 \times 10^5$ cm^{-1}).[25] We disregard any electron subband to neutral acceptor transition in the modulation-doped structure because the overlap integral of a relevant quantum-well electron envelope function with a neutral acceptor wave function is much less than the electron ground-state to hole ground-state transition.

Time-resolved measurements on these samples could provide additional experimental evidence of the different radiative lifetimes associated with the quantized optical transitions. Time-resolved measurements may also shed light on any nonradiative processes. Time-resolved measurements on AlGaN/GaN structures have been reported by several groups.[21,22] These reports show that narrow AlGaN/GaN quantum wells have shorter spontaneous radiative lifetimes than wider quantum wells due to the larger spatial overlap of the electron and hole wave functions in the narrow quantum wells.

It was recently shown that LO-phonon replicas can give rise to multiple peaks in the emission spectra in AlGaN/GaN.[28] However, one would expect that individual emission lines would be separated by the GaN LO-phonon energy which is approximately 90 meV.[29,30] In our experiments, the various PL peak-energy splittings are not 90 meV or integral multiples of 90 meV. Furthermore, the PL intensity vs energy dependence, i.e., the shape of the spectra, seen in our PL spectra is different from what one would expect from LO-phonon replicas. Replica lines become weaker with the order of the replica. We therefore do not attribute the multiline luminescence to LO phonon replicas.

To quantify the magnitude of the screening charge we compare the maximum magnitude of the optically generated areal charge σ_{opt} to the bound interface charge σ_b due to the change in total polarization across a heterointerface. Using the full width at half maximum (FWHM) of the ground-state hole wave function squared yields $\sigma_{\text{opt}} = |e| \cdot \tau_{\text{ave}}(G_{\max}) \cdot G_{\max} \cdot |\phi_{v,0}|^2_{\text{FWHM}} \approx 1.4 \times 10^{-3}$ C/m^{-2}, while $\sigma_b \approx 1.9 \times 10^{-2}$ C/m^{-2} for our $Al_{0.20}Ga_{0.80}N$/GaN SL. Therefore since $\sigma_b \gg \sigma_{\text{opt}}$, we may reasonably use the same band diagram and eigensystem for calculations at all pump intensities used in this study.

In order to verify the assignment of luminescence peaks to transitions between the quantum-confined subband states, we show in Fig. 5 the calculated transition energies relative to one of the PL spectra. The calculated transition energies range from 3.082 eV ($e_0 \rightarrow h_0$) to 3.524 eV ($e_4 \rightarrow h_0$) and clearly fall in the same energy range as the PL lines. The onset of the PL begins precisely where our calculated ground-state to ground-state transition begins. It is striking not only that luminescence occurs well above the QCSE $e_0 \rightarrow h_0$ prediction of 3.082 eV, but that the total energy spread is nearly 500 meV.

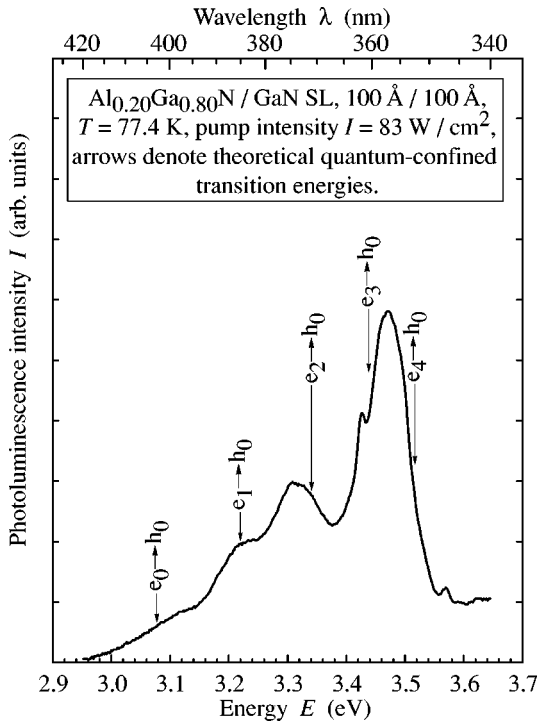

FIG. 5. Selected PL spectrum showing theoretical transition energies using theory described above. The spectrum shows clearly resolved subband transitions in excellent agreement with calculated transition energies given in Table I.

In conclusion, we have experimentally and theoretically investigated the photoluminescence properties of $Al_{0.20}Ga_{0.80}N$/GaN SL's. The PL spectra clearly show multiple, well resolved, interband transitions between quantum-confined states. We solve the Poisson-Schrödinger system of equations self-consistently to obtain the eigenfunctions, eigenenergies, and 1D band diagram in the SL. We then use this data to calculate the lifetimes, transition energies, overlap integrals squared, and the spontaneous recombination rates per unit volume for each transition between quantum-confined states. Theoretically calculated transition energies between quantum-confined states agree very well with our experimental data. Theoretically calculated spontaneous recombination rates indicate that the higher energy PL peaks should increase in intensity relative to the lower energy PL peaks as the pump intensity is increased, also in excellent agreement with our experimental data. We demonstrate that new, high-energy, transitions become observable at high pump intensities because of the increased oscillator strength of the high-energy transitions. Therefore, despite the higher energy quantum-confined states being sparsely populated compared to the lower energy states, their larger oscillator strengths allow the higher energy transitions to dominate over the lower energy transitions at high pump intensities. Our simulations also show that at high pump intensities an average spontaneous recombination lifetime in the 50 ns range can be attained even for SL's with large well and barrier widths less than $\approx$100 Å.

*Also at Physics Department, Boston University. Electronic address: ewaldron@bu.edu

†Also at Electrical and Computer Engineering Department, Boston University.

[1] G. Martin, A. Botchkarev, A. Rockett, and H. Morkoç, Appl. Phys. Lett. **68**, 2541 (1996).

[2] A. D. Bykhovski, B. L. Gelmont, and M. S. Shur, J. Appl. Phys. **81**, 6332 (1997).

[3] F. Bernardini, V. Fiorentini, and D. Vanderbilt, Phys. Rev. B **56**, 10 024 (1997).

[4] A. Hangleiter, J. S. Im, H. Kollmer, J. Off, and F. Scholz, MRS Internet J. Nitride Semicond. Res. **3**, 15 (1998).

[5] H. S. Kim, J. Y. Lin, H. X. Jiang, W. W. Chow, A. Botchkarev, and H. Morkoç, MRS Internet J. Nitride Semicond. Res. **4(S1)**, G3.3 (1999).

[6] E. L. Waldron, J. W. Graff, and E. F. Schubert, Appl. Phys. Lett. **79**, 2737 (2001).

[7] I. D. Goepfert, E. F. Schubert, A. Osinsky, P. E. Norris, and N. N. Faleev, J. Appl. Phys. **88**, 2030 (2000).

[8] P. Kozodoy, Y. P. Smorchkova, M. Hansen, H. Xing, S. P. DenBaars, U. K. Mishra, A. W. Saxler, R. Perrin, and W. C. Mitchel, Appl. Phys. Lett. **75**, 2444 (1999).

[9] S.-H. Park and S.-L. Chuang, Appl. Phys. Lett. **76**, 1981 (2000).

[10] A. Thamm, O. Brandt, J. Ringling, A. Trampert, K. H. Ploog, O. Mayrock, H. J. Wünsche, and F. Henneberger, Phys. Rev. B **61**, 16 025 (2000).

[11] M. Leroux, N. Grandjean, M. Laügt, J. Massies, B. Gil, P. Lefebvre, and P. Bigenwald, Phys. Rev. B **58**, R13 371 (1998).

[12] E. F. Schubert, W. Grieshaber, and I. D. Goepfert, Appl. Phys. Lett. **69**, 3737 (1996).

[13] I. D. Goepfert, E. F. Schubert, A. Osinsky, and P. E. Norris, Electron. Lett. **35**, 1109 (1999).

[14] J. Qu, J. Li, and G. Zhang, Solid State Commun. **107**, 467 (1998).

[15] F. Bernardini and V. Fiorentini, Phys. Rev. B **57**, R9427 (1998).

[16] N. Grandjean, B. Damilano, S. Dalmasso, M. Leroux, M. Laügt, and J. Massies, J. Appl. Phys. **86**, 3714 (1999).

[17] J. F. Nye, *Physical Properties of Crystals, their Representation by Tensors and Matrices* (Clarendon, Oxford, 1957).

[18] O. Ambacher, J. Majewski, C. Miskys, A. Link, M. Hermann, M. Eickhoff, M. Stutzmann, F. Bernardini, V. Fiorentini, V. Tilak, B. Schaff, and L. F. Eastman, J. Phys.: Condens. Matter **14**, 3399 (2002).

[19] L. W. Wong, S. J. Cai, R. Li, K. Wang, H. W. Jiang, and M. Chen, Appl. Phys. Lett. **73**, 1391 (1998).

[20] B. Gil, *Group III Nitride Semiconductor Compounds, Physics and Applications* (Oxford University, New York 1998), Chap. 5.

[21] J. S. Im, H. Kollmer, J. Off, A. Sohmer, F. Scholz, and A. Hangleiter, Phys. Rev. B **57**, R9435 (1998).

[22] J. C. Harris, T. Someya, S. Kako, K. Hoshino, and Y. Arakawa, Appl. Phys. Lett. **77**, 1005 (2000).

[23] G. H. B. Thompson, *Physics of Semiconductor Laser Devices* (John Wiley and Sons, New York, 1980).

[24] S. L. Chuang, *Physics of Optoelectronic Devices* (Wiley, New York, 1995).

[25] J. F. Muth, J. H. Lee, I. K. Shmagin, R. M. Kolbas, H. C. Casey, Jr., B. P. Keller, U. K. Mishra, and S. P. DenBaars, Appl. Phys. Lett. **71**, 2572 (1997).

[26] *Semiconductor Interfaces and Microstructures*, edited by Z. C. Feng (World Scientific, Singapore, 1992), chap. 4.

[27] S. P. Lepkowski, T. Suski, P. Perlin, V. Y. Ivanov, M. Godlewski, N. Grandjean, and J. Massies, J. Appl. Phys. **91**, 9622 (2002).

[28] G. Traetta, A. Passaseo, M. Longo, D. Cannoletta, R. Cingolani, M. Lomascolo, A. Bonfiglio, A. D. Carlo, F. D. Sala, P. Lugli, A. Botchkarev, and H. Morkoç, Physica E **7**, 929 (2000).

[29] H. Siegle, G. Kaczmarczyk, L. Filippidis, A. P. Litvinchuk, A. Hoffmann, and C. Thomsen, Phys. Rev. B **55**, 7000 (1997).

[30] Because the period of our SL is so large, interwell coupling for the states we consider is negligible and we use the term *superlattice* to simply denote the structure's periodicity.